J. Ocean Univ. China (Oceanic and Coastal Sea Research)
https://doi.org/10.1007/s11802-019-3909-3
ISSN 1672-5182, 2019 18 (3): 633-642
http://www.ouc.edu.cn/xbywb/
E-mail:xbywb@ouc.edu.cn

Transition Periods Between Sea Ice Concentration and Sea Surface Air Temperature in the Arctic Revealed by an Abnormal Running Correlation

JI Xupeng[1)], and ZHAO Jinping[1), 2), *]

1) *Key Laboratory of Physical Oceanography, Ocean University of China, Qingdao* 266100, *China*
2) *College of Oceanic and Atmospheric, Ocean University of China, Qingdao* 266100, *China*

(Received May 2, 2018; revised November 27, 2018; accepted January 21, 2019)

Abstract This study used the synthetic running correlation coefficient calculation method to calculate the running correlation coefficients between the daily sea ice concentration (SIC) and sea surface air temperature (SSAT) in the Beaufort-Chukchi-East Siberian-Laptev Sea (BCEL Sea), Kara Sea and southern Chukchi Sea, with an aim to understand and measure the seasonally occurring changes in the Arctic climate system. The similarities and differences among these three regions were also discussed. There are periods in spring and autumn when the changes in SIC and SSAT are not synchronized, which is a result of the seasonally occurring variation in the climate system. These periods are referred to as transition periods. Spring transition periods can be found in all three regions, and the start and end dates of these periods have advancing trends. The multiyear average duration of the spring transition periods in the BCEL Sea, Kara Sea and southern Chukchi Sea is 74 days, 57 days and 34 days, respectively. In autumn, transition periods exist in only the southern Chukchi Sea, with a multiyear average duration of only 16 days. Moreover, in the Kara Sea, positive correlation events can be found in some years, which are caused by weather time scale processes.

Key words Arctic; sea ice concentration; sea surface air temperature; synthetic running correlation coefficient; transition period

1 Introduction

As an important component in the Arctic, sea ice plays a critical role in the Arctic climate system. Sea ice can regulate the heat exchange between the ocean and atmosphere (Screen and Simmonds, 2010; Serreze and Barry, 2011) and modify ocean heat and freshwater contents (Sirevaag *et al*., 2011). In addition, sea ice can affect cloud and water vapor contents (Schweiger, 2004; Eastman and Warren, 2010), leading to a subsequent change in the surface energy balance (Francis and Hunter, 2006; Gorodetskaya and Tremblay, 2008; Kay *et al*., 2008). Since the late 1970s, Arctic sea ice concentration (SIC) has decreased continuously as the sea ice thickness has thinned. This decrease in SIC can be found every month, especially in September (Serreze *et al*., 2007; Comiso *et al*., 2008; Peng and Meier, 2017). The extent of sea ice cover in September 2012 reached the minimum since being recorded (Zhang *et al*., 2013). Accompanied by the dramatic decrease in sea ice, Arctic air temperatures have rapidly increased. The warming rate of the Arctic is twice as fast as that of the global average in the context of global warming (Serreze and Francis, 2006; Solomon, 2007; Screen and Simmonds, 2010; Cohen *et al*., 2014).

SIC and sea surface air temperature (SSAT) affect each other and are closely related in the process of rapid Arctic changes (Liu *et al*., 2009). Their relationship is mainly reflected in the ice-albedo feedback mechanism as follows: as air temperature rises, more sea ice melts, and the surface albedo is reduced, leading to enhanced solar energy absorption and weakened reflection, which further increases air temperature. The sea ice melting season has become longer, and the freezing time has delayed in recent years due to the interaction between sea ice and air temperature (Smith, 1998; Markus *et al*., 2009; Stroeve *et al*., 2014). As a result, the interaction between the Arctic Ocean and the atmosphere is further strengthened.

In addition to intense multiyear trends, it should be noted that the Arctic SIC and SSAT also exhibit significant seasonal variability. In winter, the SIC is high, while the SSAT is low due to a lack of solar radiation. This is the winter pattern in which the SIC and SSAT are negatively correlated. The interaction between the ocean and atmosphere is not strong due to the isolation effect of sea ice during this period. When spring comes, the air temperature increases as an effect of increased solar radiation (Overland *et al*., 1997; Serreze and Barry, 2014; Soon, 2005). The melting of sea ice exposes the open ocean to

* Corresponding author. Tel: 0086-532-66782096
E-mail: jpzhao@ouc.edu.cn

the atmosphere and leads to an increase in the absorption of solar radiation. As a result, the sensible heat content in the ocean mixed layer increases, which further enhances the melting. This period is characterized by low SIC and high SSAT, representing the summer pattern in which there is a negative correlation between SIC and SSAT. When summer ends and the sun sets, there will be plenty of heat that is transferred from the ocean back to the atmosphere. The ocean will eventually lose the extra heat from the surface mixed layer as solar radiation decreases. Then, the air temperature will fall below 0℃, and the sea ice will begin to grow (Bitz *et al*., 1996; Serreze and Barry, 2011). The summer pattern of SIC and SSAT ends and is quickly transformed into the winter pattern.

SIC and SSAT are the most basic physical parameters for measuring the changes in the Arctic climate system. It is particularly important to study the correlation between SIC and SSAT. In spring and autumn, the variations of SIC and SSAT are most intense, and the relation between them is very complicated. However, most of the previous researchers used monthly data to study the correlation between SIC and SSAT, and this caused many physical processes that occur seasonally to be ignored. Therefore, under the background of dramatic Arctic change, we aim to understand and measure the seasonally occurring changes in the Arctic climate system by analyzing the changes and correlations of Arctic SIC and SSAT during different seasons with daily data.

2 Data and Methods

2.1 Data

The daily sea ice concentration (SIC) data used here are from the Integrated Climate Date Center (ICDC), University of Hamburg, Germany. They computed the data by applying the ARTIST Sea Ice (ASI) algorithm to brightness temperatures, which are measured with the 85 GHz SSM/I and/or SSM/IS channels. Meanwhile, a 5-day median filter was applied to the entire time series to mitigate the weather effect. The time period of the original data is December 5th, 1991 until now, the spatial resolution is 12.5 km × 12.5 km (Kaleschke *et al*., 2018). The 2 m sea surface air temperature (SSAT) data are from the NCEP/NCAR reanalysis dataset, the time period of the original data is January 1st, 1948 until now with a spatial resolution of 1.875° (longitude) × 1.904° (latitude) (Kalnay *et al*., 1996).

The temporal span of all selected data is from January 1st, 1992 to December 31st, 2016. A 7-day running smoothing was applied to filter out high-frequency variations. Moreover, as the latitudinal-longitudinal grids of the SIC data and SSAT data do not match, a linear interpolation was used to interpolate the SSAT data to the same grid as the SIC data.

2.2 Correlation of SIC and SSAT

We utilize Eq. (1) to calculate the correlation coefficients of the daily SIC and SSAT (1992–2016) for every grid point and plot the coefficients over the entire Arctic Ocean, as shown in Fig.1,

$$R=\frac{\sum_{k=1}^{N}(X_k-\overline{X})(Y_k-\overline{Y})}{\sqrt{\sum_{k=1}^{N}(X_k-\overline{X})^2}\sqrt{\sum_{k=1}^{N}(Y_k-\overline{Y})^2}}, \quad (1)$$

where R is the correlation coefficients of SIC and SSAT, N represents the total days of each variable, k represents the kth sample point of each variables, X and Y represent SIC and SSAT, $\overline{X}$ and $\overline{Y}$ represent the mean values of SIC and SSAT, as shown in Eq. (2).

$$\overline{X}=\frac{1}{N}\sum_{k=1}^{N}X_k;\ \overline{Y}=\frac{1}{N}\sum_{k=1}^{N}Y_k\ . \quad (2)$$

As shown in Fig.1, SIC and SSAT show a negative correlation over most of the Arctic. Meanwhile, there is a clear regional distribution of the correlation coefficients. The negative correlation is weak in the central Arctic and areas strongly affected by the North Atlantic drift, including the Nordic Sea and western Barents Sea, while the correlation is significant at a confidence level of 99% or higher in the Arctic marginal seas.

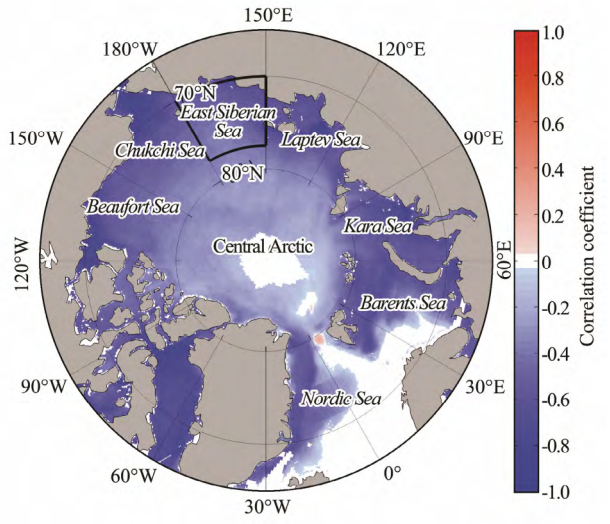

Fig.1 Correlation between SIC and SSAT over the Arctic Ocean.

2.3 Comparison of Different Running Correlation Coefficients

When analyzing the relationship between the SIC and SSAT, we can obtain the overall relationship by calculating the correlation coefficient. However, it is impossible to extract other useful information contained in the time series. In comparison, the running correlation coefficient (RCC) can reflect the entire variation process of correlation characteristics and reveal the inconsistencies between them, which is of interest in this study. Running correlation has been widely used to study other physical processes (Zhao *et al*., 2006; Ji and Zhao, 2015). The standard form is shown in Eq. (3).

$$R_r(i)=\frac{\sum_{k=i-n}^{i+n}(X_k-\bar{X}_i)(Y_k-\bar{Y}_i)}{\sqrt{\sum_{k=i-n}^{i+n}(X_k-\bar{X}_i)^2}\sqrt{\sum_{k=i-n}^{i+n}(Y_k-\bar{X}_i)^2}},$$

$$i=1+n,\cdots,N-n, \quad (3)$$

where N represents the total days of each variable, X_k represents SIC and Y_k represents the SSAT at each grid. For a time period with a running window length of $2n+1$ days, $R_r(i)$ in Eq. (3) represents the RCC of the SIC and SSAT centered over the ith running window ($i-n$, $i+n$), $\bar{X}_i$ and $\bar{Y}_i$ are local mean values of SIC and SSAT within the range of $i\pm n$, as shown in Eq. (4).

$$\bar{X}_i=\frac{1}{2n+1}\sum_{k=i-n}^{i+n}X_k;\ \bar{Y}_i=\frac{1}{2n+1}\sum_{k=i-n}^{i+n}Y_k. \quad (4)$$

This equation represents the local running correlation coefficient. Although the RCCs calculated by Eq. (3) are used extensively, there is one problem that is often ignored. When calculating the RCCs with Eq. (3), the values X_k and Y_k change within every running window, but the mean values $\bar{X}_i$ and $\bar{Y}_i$ also change. The RCCs calculated by Eq. (3) reflect only the relationship determined by variable anomalies and ignore the effect of changed local mean values on the correlation. To improve the local RCC calculation method, Zhao *et al.* (2018) proposed a new method for calculating RCCs, named the synthetic running correlation coefficient. The principle calculation method works as follows:

$$R_s(i)=\frac{\sum_{k=i-n}^{i+n}(X_k-\bar{X})(Y_k-\bar{Y})}{\sqrt{\sum_{k=i-n}^{i+n}(X_k-\bar{X})^2}\sqrt{\sum_{k=i-n}^{i+n}(Y_k-\bar{Y})^2}}$$

$$i=1+n,\cdots,N-n, \quad (5)$$

where $R_s(i)$ represents the synthetic running correlation coefficient, and other parameters are similar to those in Eq. (3), excepting that $\bar{X}_i$ and $\bar{Y}_i$ are the mean values in Eq. (2).

To determine the differences between the two RCC calculation methods, we selected the most appropriate method for our study. We randomly selected one area located in the East Siberian Sea (closed area with black lines in Fig.1) and calculated the area-averaged daily SIC and SSAT data. With an aim to remove the influence of high frequency signals, an 11-day running window was applied to calculate local and synthetic RCCs.

Fig.2a shows that there are significant seasonal variations for both SIC and SSAT. Note that SSAT data have been processed by a 7-day running smoothing to filter out high-frequency variations. In winter, when the SIC is high while the SSAT is low (vice versa in summer), there should be a significant negative correlation between SIC and SSAT. The synthetic RCCs in Fig.2c, rather than the local RCCs in Fig.2b, are consistent with the above physical processes. Changes in SIC and SSAT show high negative correlations in most of the year. Meanwhile, we find that the changes in SIC and SSAT are not always synchronized. SSAT rises rapidly while SIC exhibits little change during one period in spring, which makes the correlation coefficients of SIC and SSAT change from negative to positive values. We define the period in spring with a positive relation between SIC and SSAT as the 'spring transition period (STP)'. In addition, only the duration of more than 15 days in spring can be called STP. In spring, SSAT begins to rapidly increase due to solar radiation, but SIC remains unchanged during this time. Arctic sea ice melts after absorbing a substantial amount of radiation. It takes a long time for a rapid increase in air temperature to result in a significant melting of sea ice. The STP is caused by seasonally occurred changes in the climate system, and its physical process reveals unsynchronized variations in SIC and SSAT.

According to the above comparison, we selected a synthetic RCC calculation method to analyze the relationship between SIC and SSAT with an 11-day running window.

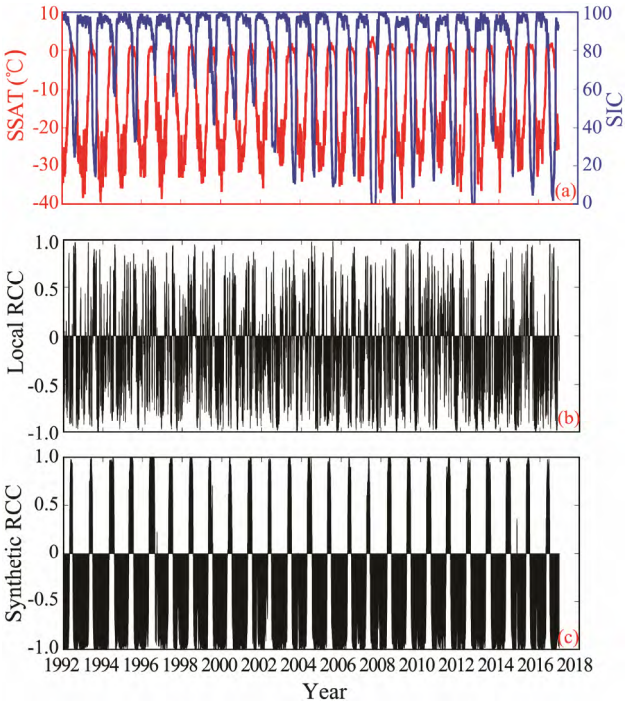

Fig.2 Changes and RCCs of SIC and SSAT for selected areas. (a) Temporal variations in SIC and SST; (b) local RCCs; (c) synthetic RCCs.

3 Overall Correlation

The research focus of this paper is the relationship between the SIC and SSAT, as well as the changing processes involved. However, the SIC variations are so weak that there is no significant correlation between the SIC and SSAT in the areas with year-round high or low SICs, so we need to exclude these areas and focus on areas where the SIC exhibits a significant seasonal change. As a result, we calculated the standard deviations of the SIC to find these areas, which are shown in Fig.3. We can see

that SIC is high and the standard deviation of SIC is small in the central Arctic, while the SIC is low and the standard deviation of the SIC is small in the areas affected by the North Atlantic drift, including the Nordic Sea and western Barents Sea. Compared with Fig.1, we can find that areas with low SIC standard deviations are also the places where SIC and SSAT are weakly related. However, SIC and SSAT show obvious negative correlation where standard deviations of the SIC are more than 15%. Areas with standard deviations of the SIC < 15% are considered the areas with weak seasonal SIC changes, where SIC and SSAT are not closely related. In the following analysis, we focus on the areas with standard deviations of the SIC > 15%.

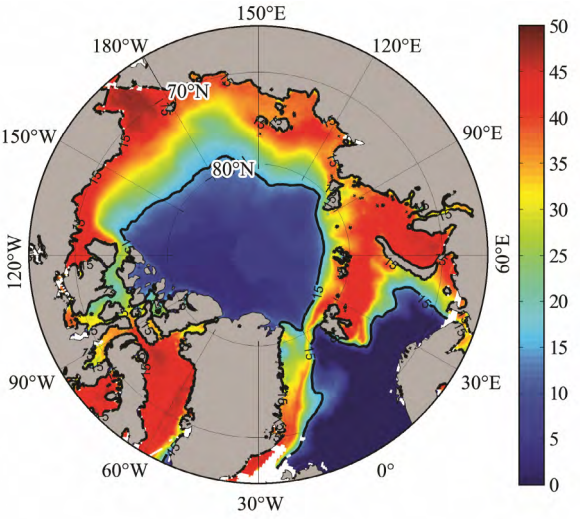

Fig.3 Standard deviations of SIC over the Arctic Ocean.

In this section, we calculated the synthetic RCCs of SIC and SSAT with an 11-day running window. We selected the RCCs and calculated the multiyear mean values for each month, as shown in Fig.4. SIC and SSAT show a negative correlation from August to April over most of the analyzed area except for the western Barents Sea and south of the Fram Strait, indicating a close relationship between sea ice melting and freezing and seasonal temperature changes in these months. However, the SIC and SSAT show a positive correlation in May and June, implying a spring transition period present in May and June over most of the analyzed area. In the spring transition period, there are two areas inconsistent with most of the analyzed area: the southern Chukchi Sea and the western Barents Sea. In these two areas, sea ice melts early and shows varying characteristics that are different from most of the Arctic Ocean.

4 Local Correlation

To describe the details of the similarities and differences in the correlations between SIC and SSAT in different regions during different time periods, we divided the analyzed area into three subregions according to the occurrence time and duration of the positive correlation between SIC and SSAT, as shown in Fig.5. The blue area represents the Beaufort-Chukchi-East Siberian-Laptev Sea (BCEL Sea), with the green area denoting the Kara Sea and the red area denoting the southern Chukchi Sea. SIC and SSAT have changed significantly in all three regions. Sea ice is mainly first-year ice in Kara Sea and southern Chukchi Sea but contains first-year ice and multi-year ice in BCEL Sea. Geographically speaking, Kara Sea belongs to a semi-enclosed area, which results in the different variation characteristics of SIC and SSAT compared with other regions. Moreover, southern Chukchi Sea is close to Pacific Ocean and affected by Pacific water.

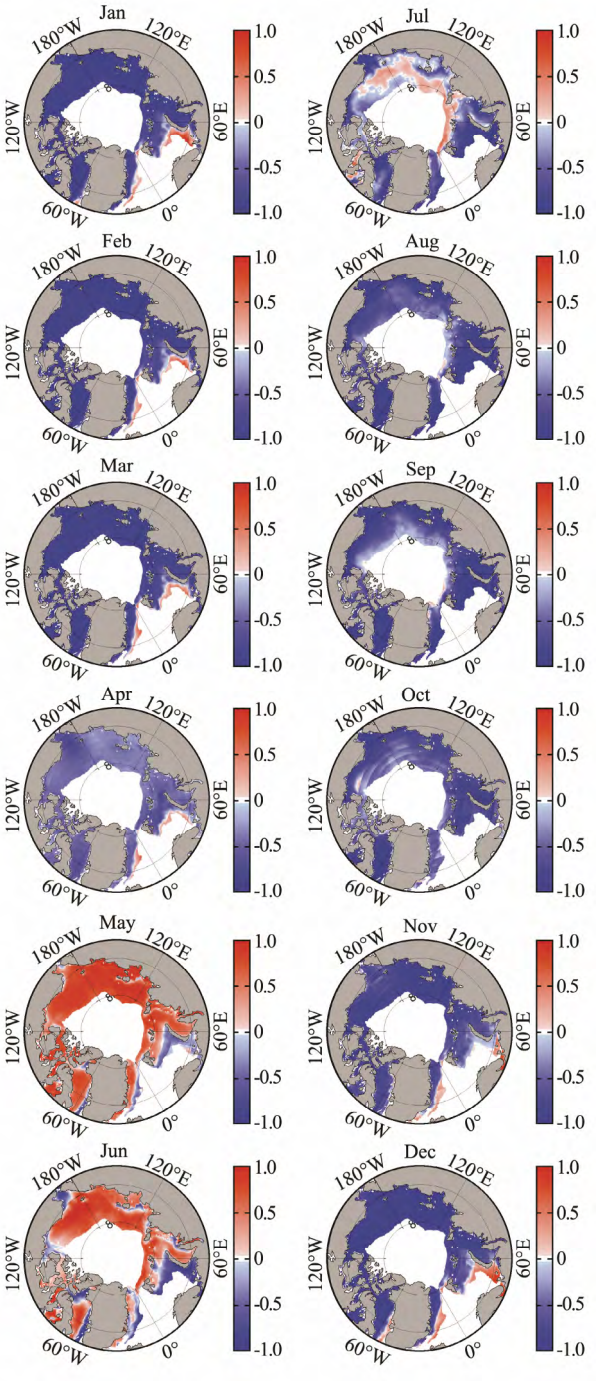

Fig.4 Monthly mean of daily RCCs between SIC and SSAT.

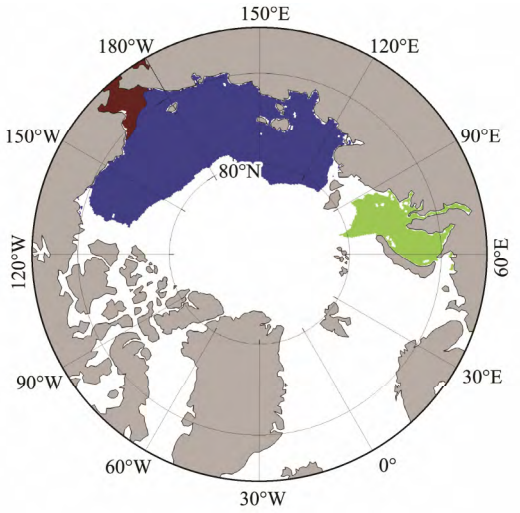

Fig.5 Regional divisions of the research area.

The regional averages of daily SIC and SSAT were calculated in every region from 1992 to 2016, and then used to calculate the daily RCCs by applying the synthetic RCC calculation method with the 11-day running window. SIC and SSAT are negatively related in all three regions (Fig.6). In the BCEL Sea and Kara Sea, positive correlation periods occur annually in spring, which reflects the STP in May and June. In the southern Chukchi Sea, aside from the STP, there is another positive correlation period in October and November, which is defined as the autumn transition period (ATP). The RCCs of SIC and SSAT are overall negative in December-March and August- September in all three regions, indicating consistency among the three regions during these six months.

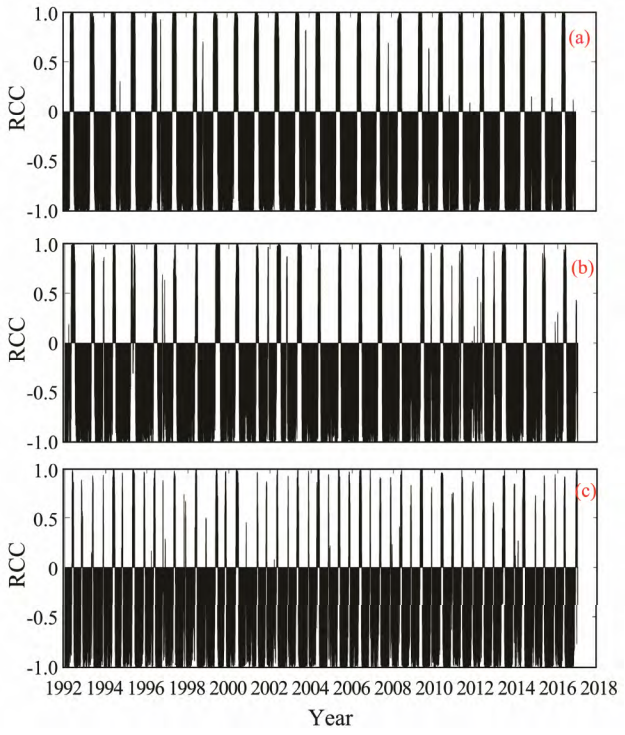

Fig.6 Daily RCCs between SIC and SSAT corresponding to (a) BCEL Sea; (b) Kara Sea; (c) southern Chukchi Sea.

The focus of this paper is to study the relationship between SIC and SSAT in each month. Taking January as an example, we will select all RCCs in January from 25-year daily RCCs and concatenate them together in chronological order. We will assess the relationship between SIC and SSAT in January over 25 years from 1992 to 2016 (Figs.7–9); then, we will analyze the interannual variations in the correlations in every region.

4.1 Spring Transition Period

The above discussions suggest that there are similarities and differences among the three regions. The characteristics of RCCs are consistent in some months but are quite different in other months. One significant difference occurs in the spring transition period (STP).

Fig.7 shows the coherently negative correlation between SIC and SSAT before April in the BCEL Sea. In April, negative and positive correlations exist simultaneously, which indicates that the correlation between SIC and SSAT changes from negative to positive beginning in April, when the STP begins. RCCs are overall positive in May and June, which is the main duration of the STP. In July, the correlation between the SIC and SSAT changes from positive to negative as the STP ends. An obvious phenomenon is that RCCs in July are almost all negative beginning in 2007, implying an earlier end of the STP.

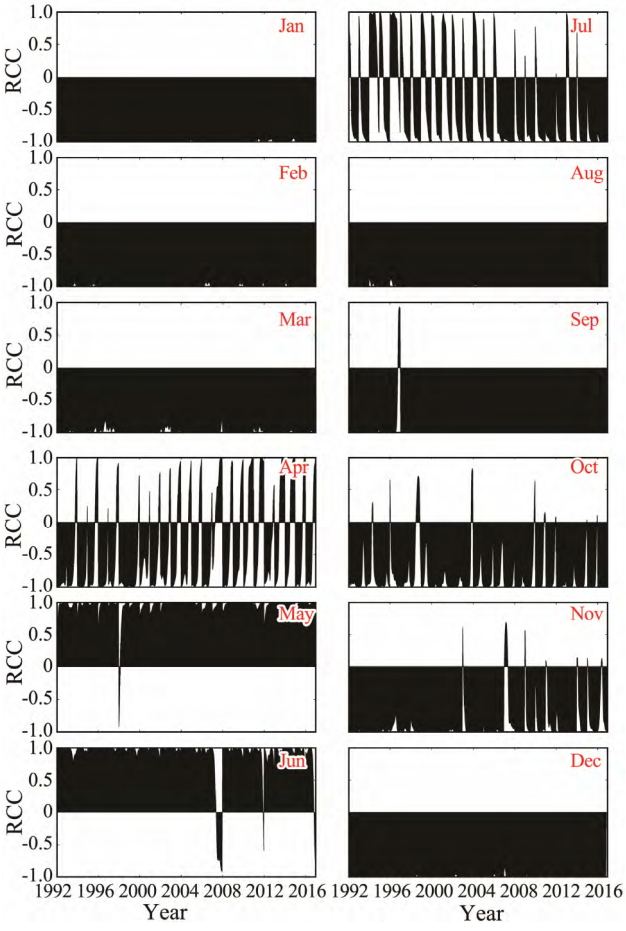

Fig.7 Daily RCCs between SIC and SSAT in every month in the BCEL Sea.

In the Kara Sea, the STP starts in April in most years. The RCCs are overall positive in May. However, the RCCs are transformed from positive to negative in June and remain negative in July (Fig.8). This result suggests that the STP mainly extends from April to June or even until July in several special years.

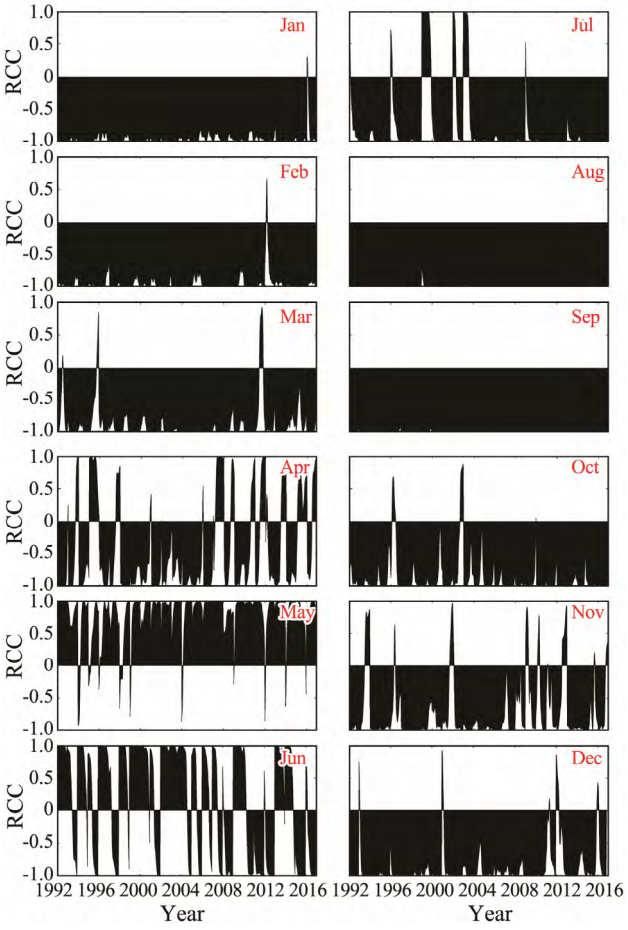

Fig.8 Daily RCCs between SIC and SSAT in every month in the Kara Sea.

The RCCs of SIC and SSAT are almost negative in April and June but are positive in May in the southern Chukchi Sea, as shown in Fig.9, illustrating that the STP lasts for only one month. This duration is different from that in the BCEL Sea and Kara Sea.

Next, we calculated the temporal characteristics of the STP. We can clearly see from the STP statistics of the BCEL Sea, Kara Sea and southern Chukchi Sea in Fig.10, where the start dates of the STP are concentrated in late April and early May. The multiyear averaged start dates are April 24, April 25 and April 30, with average durations of 74 days, 57 days and 34 days, respectively. An obvious feature is that both the start and end dates of the STP exhibit an advancing trend. The trends for the start dates of the STP in the BCEL Sea, Kara Sea and southern Chukchi Sea are −5.0 days decade^{-1}, −3.9 days decade^{-1} and −3.4 days decade^{-1}, and the trends for the corresponding end dates are −7.4 days decade^{-1}, −8.9 days decade^{-1} and −3.3 days decade^{-1}.

The above analysis indicates that the duration of the STP in the southern Chukchi Sea is the shortest among the three regions. This result is due to the geophysical location of the southern Chukchi Sea, which is the southernmost region and therefore receives the most solar radiation every spring. Moreover, the southern Chukchi Sea is affected by Pacific water, so the first-year ice is thin, which melts fastest in the spring. Therefore, the duration of sea ice existence in the southern Chukchi Sea is much shorter than that in the BCEL Sea and Kara Sea, resulting in the shortest STP in the southern Chukchi Sea.

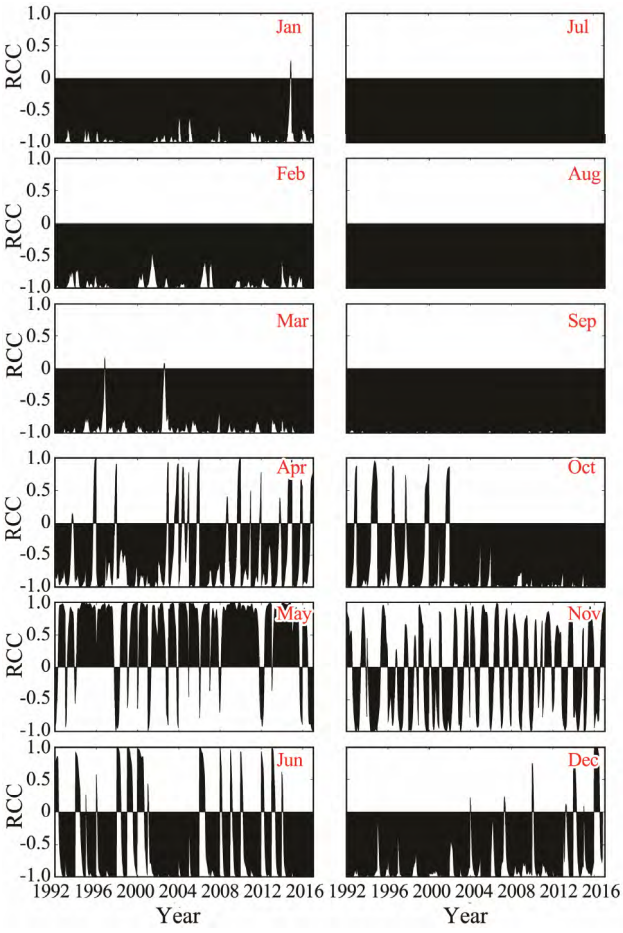

Fig.9 Daily RCCs between SIC and SSAT in every month in the southern Chukchi Sea.

4.2 Autumn Transition Period

From the above analysis, we can conclude that a STP exists in all three regions, and the duration and varying characteristics differ among these regions. In addition, there are also significant differences in October and November over these three regions, as shown in Figs.7–9. In conjunction with Fig.6, we can find two periods of positive RCCs between SIC and SSAT in the southern Chukchi Sea every year. Therefore, in addition to the STP, a positive correlation period also exists in autumn every year, and the duration of most of the positive correlations exceeds 10 days over 25 years from 1992 to 2016. As described in the previous section, we define this period as the autumn transition period (ATP).

Seasonal SIC and SSAT changes exist in autumn but differ significantly in the BCEL Sea, Kara Sea and south-

ern Chukchi Sea. Take 1993 as an example (Fig.11). In the Kara Sea, the SIC increases rapidly while the SSAT falls rapidly from 0℃ in autumn, indicating synchronized variations in SIC and SSAT, and these variations are similar to the patterns in the BCEL Sea (not shown). However, in the southern Chukchi Sea, the SIC does not increase immediately but remains low for a while when the SSAT falls rapidly from 0℃ in autumn. Similar to the physical processes of the STP, unsynchronized variations in SIC and SSAT lead to the ATP in the southern Chukchi Sea.

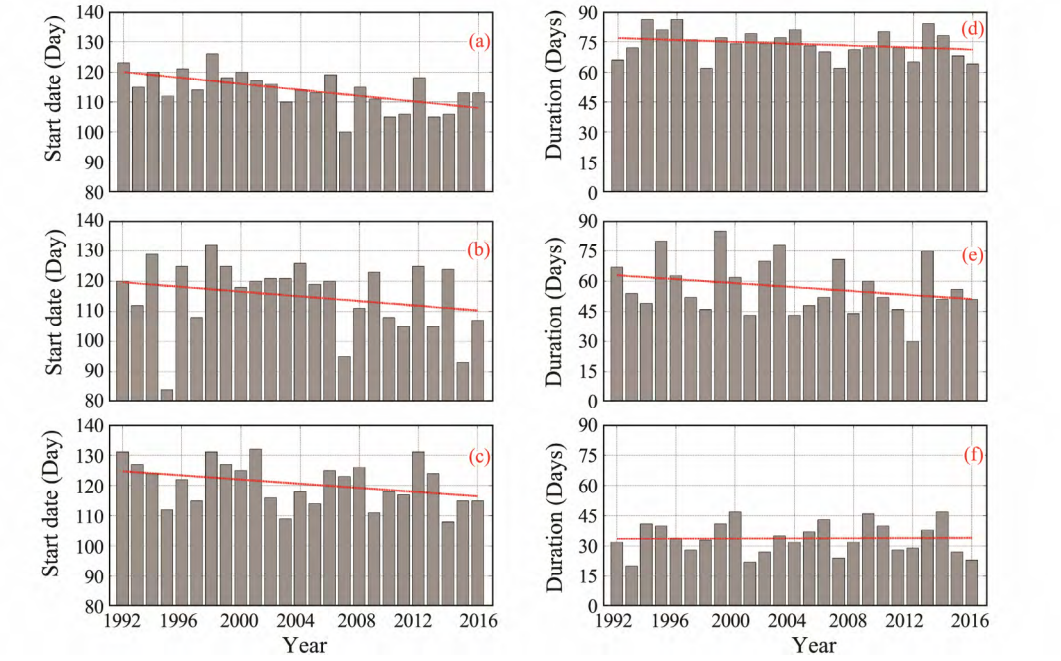

Fig.10 Start dates and durations of the STP. (a), (b) and (c) represent the start dates of the STP in the BCEL Sea, Kara Sea and southern Chukchi Sea. (d), (e) and (f) represent the durations of the STP in the corresponding regions. Red dashed lines are trend lines.

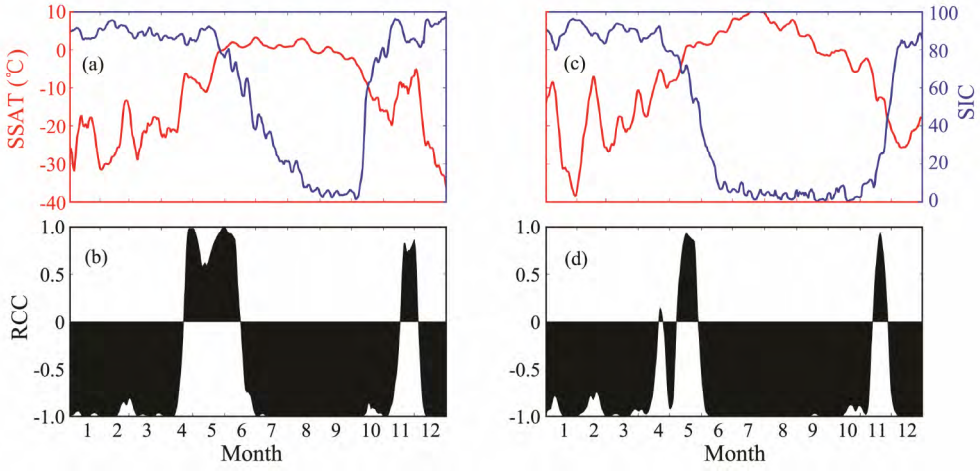

Fig.11 Changes and RCCs of SIC and SSAT in 1993. (a) and (b) are cases in the Kara Sea, (c) and (d) are cases in the southern Chukchi Sea.

We conducted a statistical analysis of the start dates and duration of the ATP in the southern Chukchi Sea. The results are shown in Fig.12. The start dates are concentrated in November, and the multiyear averaged start date is November 6, with an average duration of 16 days. In addition, there is a significant delay in the start dates of the ATP, with the ATP start dates all occurring in November since 2002. The calculated linear trends for the ATP start and end dates in the southern Chukchi Sea are 7.7 days decade^{-1} and 8.5 days decade^{-1}, respectively.

In conclusion, the ATP and STP are both caused by synchronized variations in the SIC and SSAT. However, the difference between them is that the beginning of the ATP is caused by a rapid increase in the SSAT, while the beginning of the STP is caused by a rapid decrease in the SSAT. We can learn from the specific physical processes of SIC and SSAT that they are different in spring and autumn. In spring, SSAT begins to rapidly increase due to solar radiation, but SIC remains unchanged during this time. Arctic sea ice melts after absorbing a substantial

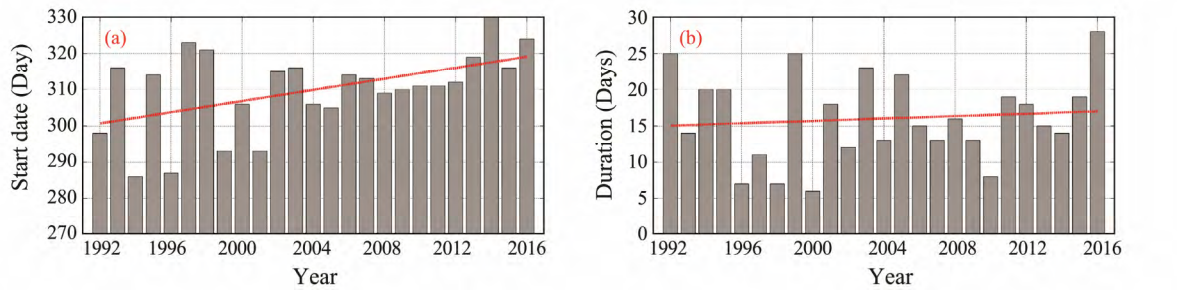

Fig.12 Start dates and durations of the ATP in the southern Chukchi Sea. (a) represents the start dates and (b) represents the durations. Red dashed lines are trend lines.

amount of radiation. It takes a long time for a rapid increase in air temperature to result in a significant melting of sea ice. In autumn, the maintenance of the SSAT mainly depends on the release of heat from the ocean to the atmosphere after the gradual disappearance of solar radiation. The SSAT will rapidly decrease, and then the ocean gradually freezes when there is no heat released from the ocean to the atmosphere. It takes only a short time for the rapid decrease in air temperature to result in a significant increase in sea ice. These processes also explain why the average duration of the ATP is only 16 days, which is far less than the 34-day average duration of the STP in the southern Chukchi Sea.

4.3 Autumn Positive Correlation Events

As shown in Figs.6–9, there is an obvious ATP every year in only the southern Chukchi Sea. The Kara Sea does not have an ATP, but this area is also different from the BCEL Sea: there are positive correlations between SIC and SSAT in autumn in some years. These events occurred in 1993, 1996, 2001, 2002, 2009, 2012 and 2016, with duration exceeding 10 days, as shown in Fig.13.

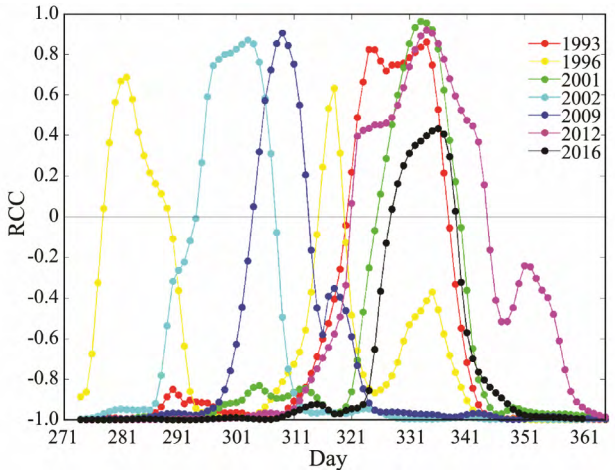

Fig.13 Autumn positive correlation events in the Kara Sea.

Fig.11 shows that the SIC increases significantly with a rapid decrease in the SSAT in the autumn of 1993 in the Kara Sea, and these changes are consistent with the seasonally occurring changes in the climate system. However, the SSAT exhibits an abnormal increase in the following period (from day 321 to day 337), while the SIC remains high because the sea ice is almost completely frozen. There is a positive correlation between the SIC and SSAT during this period. The physical processes of SIC and SSAT in this period are different from those during the ATP in the southern Chukchi Sea. The positive correlation event in autumn in the Kara Sea may be caused by the weather time scale process that induces the invasion of warm air carried by the North Atlantic warm current into the Kara Sea.

Fig.13 shows the autumn positive correlation events with positive RCCs in the Kara Sea, with positive RCCs as high as 0.8. The duration of most of the positive correlations is longer than 10 days. The highest frequencies of positive correlations are concentrated in late November and early December, and positive correlations occur earlier in some years. Among these years, 1996 is a special year when two positive correlation periods exist in autumn. In general, the synchronized variations in the autumn SIC and SSAT in the Kara Sea are attributed to the seasonally occurring variability of the climate system. However, the SSATs exhibit abnormal increases in some years due to the effects of weather processes, leading to autumn positive correlation events in the Kara Sea.

5 Conclusions

The dramatic decrease in sea ice concentration (SIC) is one of the main phenomena of rapid Arctic changes and has an impact on the global climate. Sea surface air temperature (SSAT), which represents the physical characteristics of the atmosphere, is strongly influenced by sea ice and ocean heat flux and serves as an indicator of Arctic climate change. The interaction between sea ice and air temperature can be understood by studying the correlation between the SIC and SSAT, and this information can be used to determine the effects of atmospheric processes on sea ice. A synthetic running correlation coefficient (RCC) calculation method was adopted to investigate the correlations between SIC and SSAT throughout the Arctic Ocean. The research areas are divided into three subregions, the Beaufort-Chukchi-East Siberian-Laptev Sea (BCEL Sea), Kara Sea and southern Chukchi Sea, according to the RCCs. In this paper, we analyzed the variations in the correlation between SIC and SSAT in detail in each region.

A clear spring transition period (STP) occurs every year in every region. The average start dates of the STP in the BCEL Sea, Kara Sea and southern Chukchi Sea are April 24, April 25 and April 30, with 74-day, 57-day and 34-day durations, respectively. An obvious feature is that both the start and end dates of the STP exhibit advancing trends, and the start dates exhibit trends of −5.0 days decade^{-1}, −3.9 days decade^{-1} and −3.4 days decade^{-1} in the BCEL Sea, Kara Sea and southern Chukchi Sea, and the corresponding end date trends are −7.4 days decade^{-1}, −8.9 days decade^{-1} and −3.3 days decade^{-1}.

Although STPs exist in all three regions, an obvious difference between these three regions is that the southern Chukchi Sea rather than the BCEL Sea and Kara Sea has an autumn transition period (ATP) every year. The ATP is similar to the STP and is also a result of unsynchronized variations in the SIC and SSAT caused by seasonally occurring changes in the climate system. However, the duration of the ATP is only 16 days and is far less than that of the STP, which is 34 days in the southern Chukchi Sea. Another notable feature in the southern Chukchi Sea is the trend of significant delays in the start and end dates of the ATP, which are 7.7 days decade^{-1} and 8.5 days decade^{-1}, respectively. Moreover, the SIC and SSAT in autumn are also positively correlated with each other in the Kara Sea in some years, which are caused by abnormal increases in the SSAT after the sea ice is almost completely frozen. These events are controlled by weather processes, so they do not belong to ATPs, which are controlled by seasonally occurring changes in the climate system.

Seasonal changes in the SIC and SSAT appeared over all three regions in spring and autumn in the climate system according to detailed physical processes. There are STPs in the BCEL Sea and Kara Sea, while there are both STPs and ATPs in the southern Chukchi Sea, which are controlled by seasonally occurring changes in the climate system. In addition, combining the effects of seasonally occurring changes in the climate system and weather time scale processes, positive correlation events occur in the autumn in some years in the Kara Sea.

The results of our research demonstrate a significant negative correlation between the SIC and SSAT during most months in summer and winter, reflecting the characteristics of seasonal changes and indicating synchronized variations in SIC and SSAT. In spring, the air temperature changes rapidly because of the transition of the climate system from winter to summer, but the change in sea ice lags. This synchronized variation results in a positive correlation period, which is defined as the STP. The physical process of the ATP is similar to that of the STP, except for the duration of the ATP is shorter. In terms of physical processes, seasonal transitions of the climate indeed occur during the transition period, but this kind of transition is a continuous process with start and end dates that are difficult to define. According to different change rates of sea ice and air temperature, the accurate occurrence times of the transition period are determined via a correlation analysis of sea ice and air temperature, which provides a quantitative estimate of the climate transition period and has a great impact on the understanding of sea ice change processes.

Acknowledgements

This work was supported by the National Major Science Project of China for Global Change Research (No. 2015CB953900) and the National Natural Science Foundation of China (No. 41330960).

References

Bitz, C. M., Battisti, D. S., Moritz, R. E., and Beesley, J. A., 1996. Low-frequency variability in the Arctic atmosphere, sea ice, and upper-ocean climate system. *Journal of Climate*, **9** (2): 394-408.

Cohen, J., Screen, J. A., Furtado, J. C., Barlow, M., Whittleston, D., Coumou, D., Francis, J., Dethloff, K., Entekhabi, D., Overland, J., and Jones, J., 2014. Recent Arctic amplification and extreme mid-latitude weather. *Nature Geoscience*, **7** (9): 627-637.

Comiso, J. C., Parkinson, C. L., Gersten, R., and Stock, L., 2008. Accelerated decline in the Arctic sea ice cover. *Geophysical Research Letters*, **35** (1): L01703.

Curry, J. A., Schramm, J. L., and Ebert, E. E., 1995. Sea ice-albedo climate feedback mechanism. *Journal of Climate*, **8** (2): 240-247.

Eastman, R., and Warren, S. G., 2010. Interannual variations of Arctic cloud types in relation to sea ice. *Journal of Climate*, **23** (15): 4216-4232.

Francis, J. A., and Hunter, E., 2006. New insight into the disappearing Arctic sea ice. *Eos, Transactions American Geophysical Union*, **87** (46): 509-511.

Gorodetskaya, I. V., and Tremblay, L., 2008. Arctic cloud properties and radiative forcing from observations and their role in sea ice decline predicted by the NCAR CCSM3 model during the 21st century. In: *Arctic Sea Ice Decline: Observations, Projections, Mechanisms, and Implications*. DeWeaver, E. T., ed., American Geophysical Union, Washington, D. C., 47-62.

Ji, X., and Zhao, J., 2015. Analysis of correlation between sea ice concentration and cloudiness in central Artic. *Haiyang Xuebao*, **37** (11): 92-104 (in Chinese with English abstract).

Kaleschke, L., Girard-Ardhuin, F., Spreen, G., Beitsch, A., and Kern, S., 2018. ASI Algorithm SSMI-SSMIS sea ice concentration data, originally computed at and provided by IFREMER, Brest, France, were obtained as 5-day median-filtered and gap-filled product for 1992–2016 from the Integrated Climate Date Center (ICDC, icdc.cen.uni-hamburg.de/), University of Hamburg, Hamburg, Germany. Available at: http://icdc.cen.uni-hamburg.de/1/daten/cryosphere/seaiceconcentration-asi-ssmi.html, last access: 12 January 2018.

Kalnay, E., Kanamitsu, M., Kistler, R., Collins, W., Deaven, D., Gandin, L., Iredell, M., Saha, S., White, G., Woollen, J., Zhu, Y., Leetmaa, A., Reynolds, B., Chelliah, M., Ebisuzaki, W., Higgins, W., Janowiak, J., Mo, K. C., Ropelewski, C., Wang, J., Jenne, R., and Joseph, D., 1996. The NCEP/NCAR 40-year reanalysis project. *Bulletin of the American Meteorological Society*, **77** (3): 437-471.

Kay, J. E., L'Ecuyer, T., Gettelman, A., Stephens, G., and O'Dell, C., 2008. The contribution of cloud and radiation anomalies to the 2007 Arctic sea ice extent minimum. *Geophysical Research Letters*, **35** (8): L08503.

Liu, Y., Key, J. R., and Wang, X., 2009. Influence of changes in

sea ice concentration and cloud cover on recent Arctic surface temperature trends. *Geophysical Research Letters*, **36**: L20710.

Markus, T., Stroeve, J. C., and Miller, J., 2009. Recent changes in Arctic sea ice melt onset, freezeup, and melt season length. *Journal of Geophysical Research: Oceans*, **114** (C12): C12024.

Overland, J. E., Adams, J. M., and Bond, N. A., 1997. Regional variation of winter temperatures in the Arctic. *Journal of Climate*, **10** (5): 821-837.

Peng, G., and Meier, W. N., 2017. Temporal and regional variability of Arctic sea-ice coverage from satellite data. *Annals of Glaciology*, **59**: 191-200.

Screen, J. A., and Simmonds, I., 2010. Increasing fall–winter energy loss from the Arctic Ocean and its role in Arctic temperature amplification. *Geophysical Research Letters*, **37** (16): L16707.

Schweiger, A. J., 2004. Changes in seasonal cloud cover over the Arctic seas from satellite and surface observations. *Geophysical Research Letters*, **31** (12): L12207.

Serreze, M. C., and Barry, R. G., 2011. Processes and impacts of Arctic amplification: A research synthesis. *Global and Planetary Change*, **77** (1-2): 85-96.

Serreze, M. C., and Barry, R. G., 2014. *The Arctic Climate System*. Cambridge University Press, Cambridge, 51-53.

Serreze, M. C., and Francis, J. A., 2006. The Arctic amplification debate. *Climatic Change*, **76** (3-4): 241-264.

Serreze, M. C., Holland, M. M., and Stroeve, J., 2007. Perspectives on the Arctic's shrinking sea-ice cover. *Science*, **315** (5818): 1533-1536.

Sirevaag, A., Rosa, S. D. L., Fer, I., Nicolaus, M., Tjernström, M., and McPhee, M. G., 2011. Mixing, heat fluxes and heat content evolution of the Arctic Ocean mixed layer. *Ocean Science Discussion*, **7** (3): 335-349.

Smith, D. M., 1998. Recent increase in the length of the melt season of perennial Arctic sea ice. *Geophysical Research Letters*, **25** (5): 655-658.

Solomon, S., 2007. *Climate Change 2007 – The Physical Science Basis: Working Group I Contribution to the Fourth Assessment Report of the IPCC*. Vol. 4. Cambridge University Press, Cambridge, 996-997.

Soon, W. W. H., 2005. Variable solar irradiance as a plausible agent for multidecadal variations in the Arctic–Wide surface air temperature record of the past 130 years. *Geophysical Research Letters*, **32** (16): L16712.

Stroeve, J. C., Markus, T., Boisvert, L., Miller, J., and Barrett, A., 2014. Changes in Arctic melt season and implications for sea ice loss. *Geophysical Research Letters*, **41** (4): 1216-1225.

Zhang, J., Lindsay, R., Schweiger, A., and Steele, M., 2013. The impact of an intense summer cyclone on 2012 Arctic sea ice retreat. *Geophysical Research Letters*, **40** (4): 720-726.

Zhao, J., Cao, Y., and Shi, J., 2006. Core region of Arctic oscillation and the main atmospheric events impact on the Arctic. *Geophysical Research Letters*, **33** (22): L22708.

Zhao, J., Cao, Y., and Wang, X., 2018. The physical significance of the synthetic running correlation coefficient and its applications in oceanic and atmospheric studies. *Journal of Ocean University of China*, **17** (3): 451-460.

(Edited by Chen Wenwen)